Chemical Science

Accepted Manuscript

This article can be cited before page numbers have been issued, to do this please use: K. Yu, Y. Lv, Y. Li, Z. Wang, S. Zhang, J. Wei, S. Xue, C. Wang and B. Yang, *Chem. Sci.*, 2025, DOI: 10.1039/D5SC06557G.

ROYAL SOCIETY OF CHEMISTRY

rsc.li/chemical-science

DOI: 10.1039/D5SC06557G

Realizing Highly Efficient Electro-Fluorescence with Co-axial Hybrid Local and Charge-transfer (HLCT) Excited State

Kuo Yu [1], Yingbo Lv [1], Yilong Li [1, 2], Zirui Wang [1], Shi-Tong Zhang [1,], Jinbei Wei [2,*], Shanfeng Xue [3,*], Chenguang Wang[2] and Bing Yang[1]*

1 State Key Laboratory of Supramolecular Structure and Material, College of Chemistry, Jilin University, Changchun, 130012, P. R. China

2 State Key Laboratory of Integrated Optoelectronics (JLU Region), College of Electronic Science and Engineering, Jilin University, Changchun, 130012, China

3 Key Laboratory of Rubber-Plastics of the Ministry of Education, School of Polymer Science & Engineering, Qingdao University of Science and Technology, 53 Zhengzhou Road, Qingdao 266042, P. R. China

Email: stzhang@jlu.edu.cn, jinbwei@jlu.edu.cn, sfxue@qust.edu.cn

Abstract

In this work, we report two high-performance donor-acceptor (D-A) electro-fluorescent materials DPXZ-PI and DPXZ-PICN with novel co-axial hybrid local and charge-transfer (HLCT) excited state design method. Featuring the direct bonding of strong electron donor diphenoxazine (DPXZ) and weak electron acceptor phenanthroimidazole (PI), the co-axial HLCT state is initially constructed in DPXZ-PI with high photoluminescence quantum yield (PLQY) of 81.7% and a high maximum external quantum efficiency (EQE) of 14.8% in doped organic light-emitting diode (OLED), which is among the best results of the HLCT emitter-based OLEDs. Notably, the co-axial HLCT state is robust upon the introduction of strong electron acceptor cyano-benzene, which allows the increasing of electron mobility in OLED and high EQE of 11.6% in non-doped OLED of DPXZ-PICN. Overall, the co-axial HLCT realizes the increasing of PLQY with maintained exciton utilizing efficiency (EUE) in OLED, which is an effective method for highly-efficient electro-fluorescent materials and devices.

Key words: OLED; HLCT; spin-statistics; excited state; EQE.

View Article Online
DOI: 10.1039/D5SC06557G

1. Introduction

Organic light-emitting diode (OLED) technology represents a critical research direction in optoelectronic materials and devices due to its broad application prospects in solid-state lighting, flexible displays and sensors. However, conventional fluorescent OLEDs can only utilize the electrically generated 25% singlet excitons (S_1), while the 75% triplet excitons (T_1) are dissipated *via* non-radiative decay.[1] To circumvent this fundamental spin-statistics limit and achieve a 100% exciton utilization efficiency (EUE) in the low-cost electro-fluorescence, researchers have proposed diverse exciton harvesting strategies, including triplet-triplet annihilation (TTA)[2-6], thermally activated delayed fluorescence (TADF)[7-31], hybrid local and charge-transfer (HLCT)[32-47] and stable doublet state. Especially, charge-transfer (CT) excited state makes the difference on the triplet harvesting, because that CT state can reduce the singlet-triplet energy gap by lowering the degree of orbital overlap, thereby completely converting the electro-generated triplet excitons into singlet excitons. Furthermore, adequate spin-orbit coupling (SOC) coefficient can accelerate the reversed intersystem crossing (RISC) by the incorporation of LE component to adapt to the parity selection rule for RISC (known as the El-Sayed rule), which is becoming the basic principle of the TADF and HLCT mechanisms.[48,49]Between them, the HLCT mechanism offers distinct advantages such as short excited-state lifetimes, suppressed efficiency roll-off and high external quantum efficiency (EQE) in non-doped devices. In 2012, Li et al. reported the first blue-emitting HLCT material based on a triphenylamine-phenanthroimidazole (TPA-PPI) framework, achieving a breakthrough beyond the spin-statistics limit, however, the realized EUE remained limited to merely 28% due to the relatively weak CT character.[32] Subsequently, in 2015, Zhang et al. significantly advanced this approach. By introducing a perpendicular cyano-group substituent onto the TPA-PPI backbone, they engineered an orthogonal HLCT construction with strong CT character. This modification dramatically increased the EUE to near 98%, concurrently demonstrating that the CT component within the HLCT state is crucial for the complete harvesting of electrically generated triplets. The resulting OLED achieved a record-setting EQE of 7.8%, representing the highest reported EQE for non-doped

blue OLEDs at that time. [47] Most recently, pioneering works by Tang and Wang et al. further demonstrated the superior properties and potential of orthogonal HLCT materials by constructing a cross-axis configuration, which achieved high-performance, multifunctional OLEDs.[50] However, the orthogonal HLCT still remains problem in terms of the strong CT character, which can lead to a significant reduction in PLQY due to its intrinsic property of low-orbit overlap, thereby fundamentally limiting the upper bound of the EQE according to the following relation:

$$EQE = \eta_{e-h} \cdot PLQY \cdot \eta_{out} \cdot EUE$$

Where $\eta_{e\text{-}h}$ represents the exciton recombination efficiency, in structurally optimized OLEDs, this value should ideally approach 100%; η_{out} represents the light-outcoupling efficiency, which is estimated as 20% ~ 30% in the glass-substrate bottom-emissive OLED depending on the micro-structural regularity of the functional layers in OLED. For example, the above mentioned orthogonal HLCT material TBPMCN exhibits a PLQY of merely 40%, and the upper-limit of EQE is only 8% when the η_{out} is estimated as 20%. Therefore, innovative molecular design that can substantially enhance the PLQY while preserving proper CT property for full EUE is needed.

In this work, we employ a direct linkage between a strong electron donor diphenoxazine (DPXZ) and a weak electron acceptor phenanthroimidazole (PI) to limit the CT transition and LE transition to be in the same direction, and construct a novel co-axial HLCT excited state. According to this molecular design method, two highly efficient emitter DPXZ-PI and DPXZ-PICN are synthesized and investigated. The co-axis HLCT materials exhibit nearly doubled PLQY comparing to the orthogonal HLCT materials, which boosted the EQE to 14.8% (doped OLED of DPXZ-PI) and 11.6% (non-doped OLED of DPXZ-PICN). This comparative result unequivocally demonstrates that the co-axial molecular design strategy constitutes a novel approach for achieving high exciton utilization via the CT state while simultaneously realizing a significantly boosted PLQY, ultimately leading to exceptional EQE.

View Article Online
DOI: 10.1039/D5SC06557G

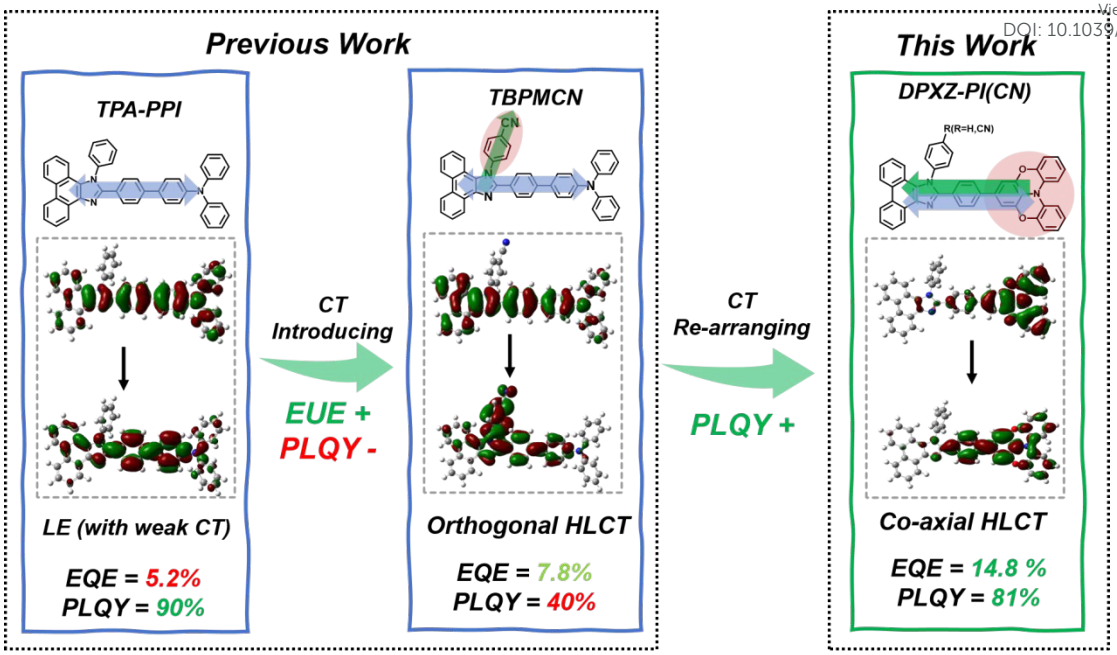

Scheme 1 Schematic excited state design method, photophysical performance and OLED performance of the weak-CT HLCT, orthogonal HLCT and co-axial HLCT materials.

2. Results and Discussions

2.1 Molecular Design

We firstly carried out density functional theory (DFT) and time-dependent DFT (TDDFT) calculations under m062x/6-31g (d, p) level to obtain the optimized geometries of S_0 and S_1 states of DPXZ-PI and DPXZ-PICN, along with their excitation energies and visualized natural transition orbitals (NTOs) to illustrate the excited state property of the co-axial HLCT state (Figure 1). As depicted in Scheme 1, the orthogonal HLCT material TBPMCN shows two distinguishable transitions with orthogonal distribution: the LE-like transition at the triphenylamine (TPA)-PI backbone (which is similar to that of TPA-PPI), and the CT-like transition from the TPA-PI backbone donor to the perpendicular cyano-benzene acceptor. In the case of DPXZ-PI and DPXZ-PICN, the combination of the strong electron-donating ability of the DPXZ moiety and the relatively weak electron-accepting ability of PI firstly results in a pronounced CT transition character from DPXZ to the imidazole ring. More evidently, the spatial

View Article Online
DOI: 10.1039/D5SC06557G

overlap between the S_1 NTO "hole" and "electron" of DPXZ-PI and DPXZ-PICN can be observed within the DPXZ donor and adjacent phenyl ring, which is consistent with the relatively high oscillator strength of the S_1 excited states (f = 0.7365 for DPXZ-PI and f = 0.6983 for DPXZ-PICN, respectively). This transition character seems to be similar to the previously reported HLCT material TPA-PPI (Scheme 1), which represents a relatively weak CT character, yet the strong donor ability of DPXZ in DPXZ-PI and DPXZ-PICN involves more n→π* transition or CT transition component, which is identical to their decreased oscillator strength comparing to TPA-PPI. More importantly, this stronger CT character will no doubt lead to more efficient triplet harvesting. As shown in Figure 1a, the T_3 and T_2 energy levels of DPXZ-PI and DPXZ-PICN are close to their S_1 energy level, and large energy gaps of > 0.7 eV are observed between the T_2 and T_1 energy levels, forming a typical "hot-exciton" channel. Furthermore, the SOC coefficients between the S_1 and T_3 energy levels of DPXZ-PI and DPXZ-PICZ are all large enough (0.61 cm^{-1} and 0.48 cm^{-1} for DPXZ-PI and DPXZ-PICN, respectively, Table 1) for the high-lying reversed intersystem crossing (hRISC). This result obeys the El-Sayed rule that RISC is more efficient for the transition from n→π* states to π→π* states (Figure S2), [51-54] owing to the HLCT property of the S_1 excited states of DPXZ-PI and DPXZ-PICN that the LE component can provide certain $\pi\rightarrow\pi^*$ transition property. Strikingly, different from our previous works [32, 47], cyano-substitution at the phenyl-side-group of DPXZ-PI (yielding DPXZ-PICN) results in no significant difference on its NTO, revealing that the co-axial HLCT is robust upon substitution of strong acceptor, which can potentially give rise to the electron injection and transportation in OLED without severe PLQY reduction.

View Article Online
DOI: 10.1039/D5SC06557G

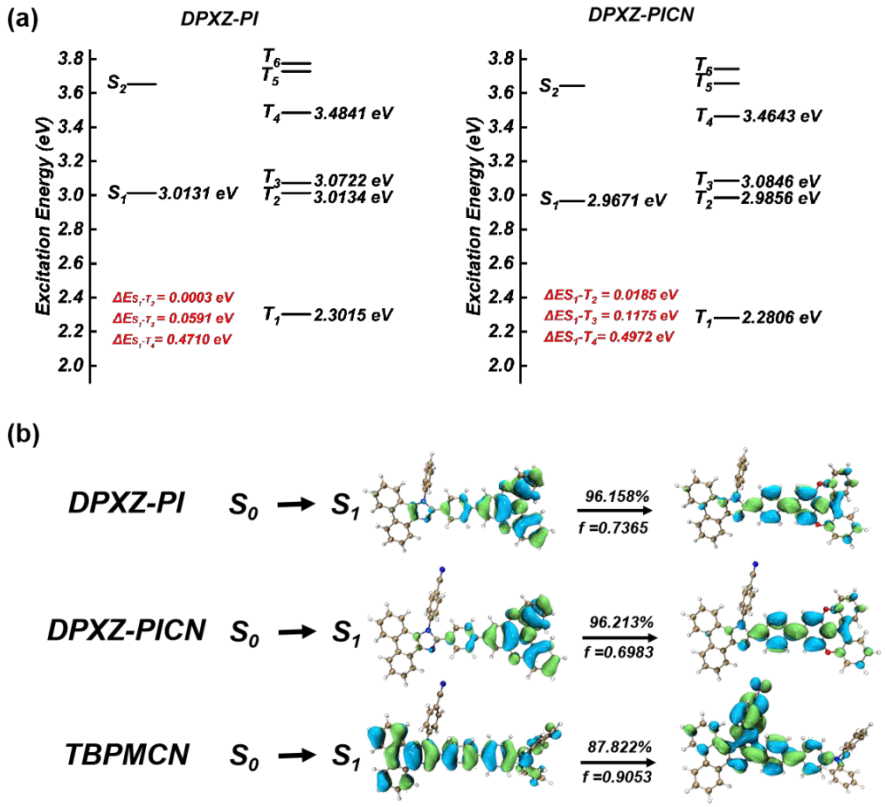

Figure 1 (a) Excitation energy diagrams of DPXZ-PI and DPXZ-PICN;(b) $S_0 \rightarrow S_1$ NTO of DPXZ-PI, DPXZ-PICN and TBPMCN. The geometry optimization and excites state estimation are carried out using a Gaussian 16 A.03 package[55] under m062x/6–31 g d, p) and td-m062x/6-31 g (d, p) level, respectively. The natural transition orbital (NTO) images are generated using a MultiWFN 3.8 dev package.[56] The SOC coefficient is calculated using a Beijing Density Function (BDF) package under td-m062x/6–31 g (d, p) level.[57-60]

Table 1 SOC coefficients related to the S_1 state of DPXZ-PI and DPXZ-PICN.

	DPXZ-PI	DPXZ-PICN
S_1-T_1	0.10 cm^{-1}	0.09 cm^{-1}
S_1-T_2	0.12 cm^{-1}	0.19 cm^{-1}
S_1-T_3	0.61 cm^{-1}	0.48 cm^{-1}
S_1-T_4	0.22 cm^{-1}	0.30 cm^{-1}
S_1-T_5	0.29 cm^{-1}	0.45 cm^{-1}
S_1-T_6	0.54 cm^{-1}	0.36 cm^{-1}

View Article Online
DOI: 10.1039/D5SC06557G

Beyond the radiative decay ability, the non-radiative decay rate constitutes another critical factor governing the PLQY of materials. Consequently, upon frequency calculations, we further analyzed the reorganization energy projections onto all normal vibrational modes as well as their Huang-Rhys factors (HR factors or S) for both DPXZ-PI and DPXZ-PICN. For comparative analysis, identical calculations were performed on the two reported benchmark structures in Scheme 1, that is, the weak-CT structure TPA-PPI and the strong-CT structure TBPMCN. Our analysis reveals that while the vibrational modes contributing significantly to the total reorganization energy exhibit similar distributions across all four materials, their relative strengths show distinct differences. As illustrated in Figure 2, the dominant reorganization energy contribution of the orthogonal-direction HLCT material TBPMCN arises from a low-frequency mode at 151.95 cm^{-1}. This mode corresponds to the torsional vibration of the peripheral benzonitrile substituent relative to the TPA-PPI conjugated core. In stark contrast, the maximum reorganization energy contributions of the weak-CT or the co-axial-direction HLCT structures (TPA-PPI, DPXZ-PI and DPXZ-PICN) occur at higher frequencies (TPA-PPI: 1702.75 cm^{-1}; DPXZ-PI: 1752.95 cm^{-1}; DPXZ-PICN: 1751.03 cm^{-1}). These modes primarily involve the C-C stretching vibrations of the TPA-PI or DPXZ-PI backbone. This disparity aligns fundamentally with their distinct HLCT architectures: the vibrational modes dominating the reorganization energy are intrinsically linked to the D-A connectivity and the specific composition of the HLCT state. These results are identical to the similar NTOs of DPXZ-PI and DPXZ-PICN as well as the calculated CT component results on different directions (Table S1), where the CT ratios of DPXZ-PI and DPXZ-PICN on the co-axis direction are obviously larger than those at orthogonal direction. Critically, these HLCT-architecture-dependent vibrational modes directly govern their respective non-radiative decay rates. As shown in Figure 2, the HR factor associated with the key C-C twisting mode at 151.95 cm^{-1} in TBPMCN is substantial (S = 4.38173). Conversely, the HR factors of the analogous high-frequency modes in the other three materials are orders of magnitude lower, demonstrating

View Article Online
DOI: 10.1039/D5SC06557G

their significantly suppressed non-radiative decay rates compared to the strong CT structure TBPMCN. Consequently, even if the oscillator strength of the co-axial HLCT state is slightly lower, its inhibited non-radiative pathways enable the realization of high luminescence efficiency from the excited state. Furthermore, the DPXZ structure with two incorporated ether oxygen bridge, effectively suppresses the phenyl ring vibrations compared to TPA, contributing positively to the reduction of non-radiative decay. Finally, comparing the total reorganization energies of the four materials (TBPMCN: 3356.87 cm^{-1}; TPA-PPI: 2929.56 cm^{-1}; DPXZ-PI: 2739.20 cm^{-1}; DPXZ-PICN: 2763.67 cm^{-1}), the strong CT structure TBPMCN exhibits the highest total reorganization energy, and the co-axial HLCT materials DPXZ-PI, DPXZ-PICN possess even lower total reorganization energies than the weak-CT structure TPA-PPI. Overall, the co-axial HLCT materials can facilitate higher PLQY due to the suppressed non-radiative transition profiles. The last but not the least, different from the sharp change of cyano-substitution from TPA-PPI to TBPMCN, the cyano-substitution on DPXZ-PI does not makes any obvious change on the dominate vibration modes, which is also the evidence that the co-axial HLCT is robust upon functional group modification.

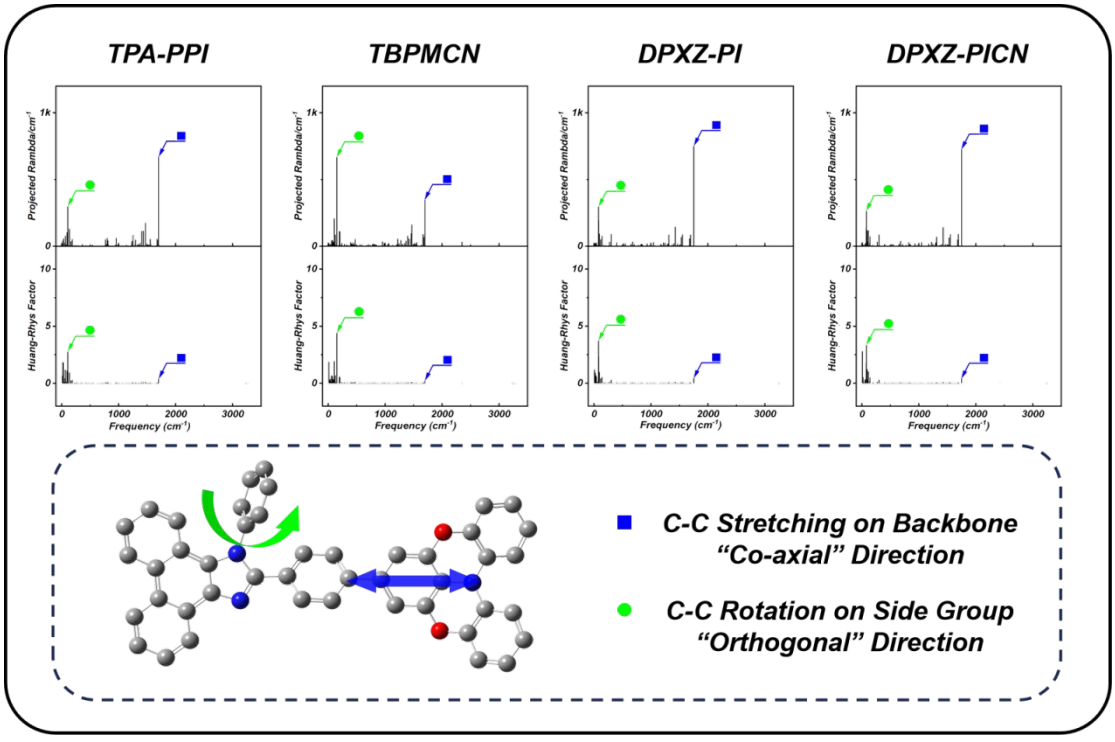

Figure 2 Projected re-organization energy, Huang-Rhys factor and corresponding

View Article Online
DOI: 10.1039/D5SC06557G

vibrational modes of TPA-PPI, TBPMCN, DPXZ-PI and DPXZ-PICN. The calculations are carried out using a Gaussian 16 A.03 package and a molecular materials property prediction package (MOMAP).[61-66]

2.2 Excited State Properties

The synthesis details of DPXZ-PI and DPXZ-PICN are described at the supporting information. We measured the absorption and emission spectra of the DPXZ-PI and DPXZ-PICN molecules (Figure 3a, Figure S5 and Figure S6). In contrast to the classic orthogonal-direction HLCT material TBPMCN, both DPXZ-PI and DPXZ-PICN exhibit two distinct absorption bands, centered near 330 nm and 370 nm, respectively. Based on the characteristic absorption profiles of HLCT materials like TBPMCN, the band around 370 nm can be assigned to the HLCT absorption. The isolated peak at 330 nm also possesses a relatively high molar extinction coefficient. However, this feature cannot be attributed solely to a polycyclic π-π* transition, which would locate at around 280 nm. Considering the well-matched electronic properties of the strong DPXZ donor and the weak PI acceptor, the absorption near 330 nm is likely intrinsic to the DPXZ unit itself, consistent with the S_2 NTO of DPXZ-PI. The absorption spectrum of DPXZ-PICN is broadly similar to that of DPXZ-PI, differing primarily in the less resolved distinction between its two absorption bands, resulting in a single broad absorption peak. Solvatochromic emission spectra provide more critical insights into the nature of the HLCT state. For TPA-PPI and TBPMCN, the introduction or absence of cyano group profoundly alters HLCT formation, dramatically affecting peak shape, spectral width, and the magnitude of solvatochromic shift. However, the co-axial HLCT materials DPXZ-PI and DPXZ-PICN exhibits very little difference beyond an about 5 nm disparity in solvatochromic shift. Both DPXZ-PI and DPXZ-PICN display pronounced vibrational fine structure in non-polar hexane and significant spectral broadening in higher polarity solvents(Figure 3b). Their Lippert-Mataga model of the two materials further reveal comparable, one-component lines, corresponding to the excited-state dipole moments of 18.8 Debye and 19.9 Debye for DPXZ-PI and DPXZ-PICN, respectively (Figure 3c). This

observation reinforces the concept of a robust co-axial HLCT character largely unaffected by peripheral cyano substitution. Furthermore, both materials exhibit single-exponential nanosecond-scale fluorescence decays in dilute solution(Figure 3d), and their distinct phosphorescence emission(Figure 3e), resolvable from the fluorescence, are detectable at liquid nitrogen temperature (77 K). The phosphorescence maxima occur at 542.6 nm for DPXZ-PI and 541.2 nm for DPXZ-PICN, corresponding to large singlet-triplet energy gaps (ΔE□□) of 0.6392 eV and 0.607 eV respectively, which unequivocally demonstrate their typical HLCT characteristic.

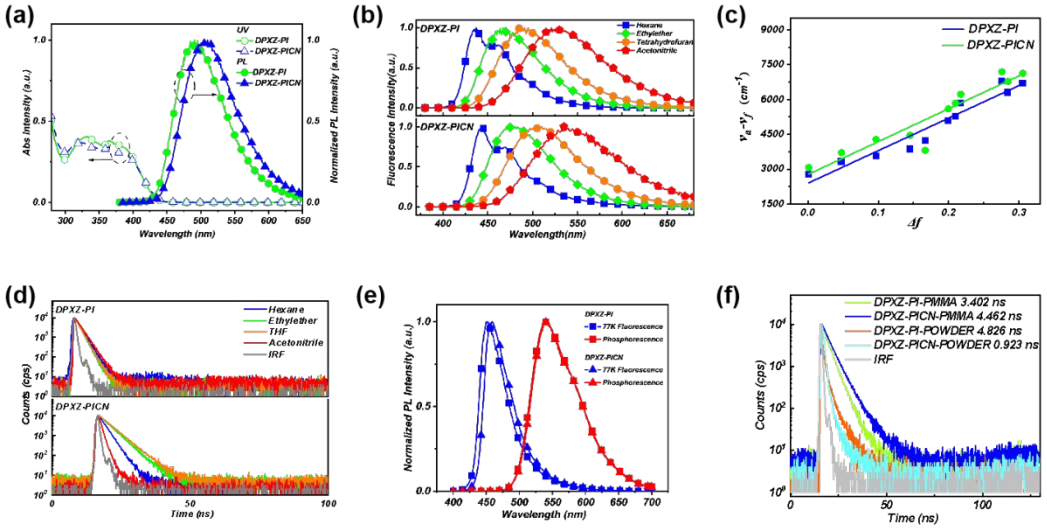

Figure 3 Photophysical properties of DPXZ-PI and DPXZ-PICN. (a) absorption and emission spectra in THF diluted solution (b) solvatochromic emission spectra in hexane, ethyl-ether, THF and acetonitrile diluted solutions (c) Lippert-Mataga solvatovhromic model (d) nanosecond-level lifetime in hexane, ethyl-ether, tetrahydrofuran and acetonitrile diluted solutions (e) fluorescence and phosphorescence under 77 K (f) nanosecond-level lifetime in non-doped powder and PMMA doped film. The concentration of the diluted solutions is 1×10^{-5} M.

A key advantage of the HLCT state lies in its elevated radiative decay rate constant (k_r) and suppressed non-radiative decay rate constant (k_{nr}) within moderate polarity environments, enabling high PLQYs in aggregates. This property constitutes the foundation for achieving high electroluminescence efficiency. As summarized in Table

View Article Online
DOI: 10.1039/D5SC06557G

2, both DPXZ-PI and DPXZ-PICN exhibit substantial k_r values in moderate polarity solvents (ethyl-ether and tetrahydrofuran (THF)) comparing to those in the low-polarity solvent hexane and concurrently, the corresponding k_{nr} are significantly suppressed. This behavior highlights the beneficial characteristic of the LE excited state property, which effectively mitigates non-radiative decay even in relatively polar environments. This advantage derives a hopeful result that both DPXZ-PI and DPXZ-PICN achieve high PLQY of 81.7% and 83..9% respectively in 1% doped films in polymethyl methacrylate (PMMA), being approximately two-fold and 1.75-fold that of TBPMCN, respectively, meaning that if the EUEs of the DPXZ-PI and DPXZ-PICN based OLED can be preserved as near 100%, the EQEs can be the same-folds to the TBPMCN based OLED. Additionally, the introduction of the cyano group in DPXZ-PICN leads to a dramatic increase on k_{nr} only within high polar solvent acetonitrile, which indicates that pronounced CT character of the co-axial HLCT could only be induced under extremely high polarity conditions, revealing to its robustness under different circumstances.

Table 2 Excited state dynamics of DPXZ-PI and DPXZ-PICN.

Solvent	DPXZ-PI				DPXZ-PICN			
	PLQY(%)	τ(ns)	k_r (10^8 s^{-1})	k_{nr} (10^8 s^{-1})	PLQY(%)	τ(ns)	k_r (10^8 s^{-1})	k_{nr} (10^8 s^{-1})
Hexane	60.7	1.904	3.19	2.06	36.1	2.023	1.78	3.16
Ethylether	60.3	3.321	1.82	1.20	58.6	3.376	1.74	1.23
THF	53.4	3.482	1.53	1.34	60.4	3.740	16.1	1.06
Acetonitrile	23.5	4.208	0.60	1.82	4.3	0.810	0.50	11.8
PMMA	81.7	3.402	2.40	0.54	83.9	4.462	1.58	0.66
Neat film	100	4.826	0.65	1.42	30.2	0.923	0.61	10.2

2.3 OLED Performances

Besides high PLQY, efficient charge carrier transport is also crucial for realizing

View Article Online
DOI: 10.1039/D5SC06557G

higher-efficiency OLEDs. Prior to OLED fabrication, we characterized the carrier mobility of DPXZ-PI and DPXZ-PICN by constructing and analyzing hole-only devices (HODs) and electron-only devices (EODs) using the space charge limited current (SCLC) method. On the one hand, due to the weak electron acceptor ability of PI group, the average electron mobility (μ_{ele}) of DPXZ-PI is estimated to be 1.86×10^{-6} cm^2 V^{-1} s^{-1}, which is a modest value for organic emitters. DPXZ-PICN exhibited a doubled average μ_{ele} of 3.78×10^{-6} cm^2 V^{-1} s^{-1}, which can be assigned to the introducing of the electron acceptor cyano group. On the other hand, both of the two materials demonstrate significantly higher hole mobilities (μ□): DPXZ-PI and DPXZ-PICN achieved an average μ□ of 1.56×10^{-4} cm^2 V^{-1} s^{-1} and 3.79×10^{-4} cm^2 V^{-1} s^{-1}respectively. Therefore, despite their moderate electron mobilities, the excellent hole-transport capabilities of both materials suggest that high electroluminescence efficiency and low efficiency roll-off remain achievable through rational host matrix selection and optimized doping concentrations in device architectures. Next, electroluminescent (EL) materials must possess excellent thermal stability to ensure they do not decompose (reflected by the thermal decomposition temperature, T_d) or suffer from morphology degradation (reflected by the glass transition temperature, T_g) during device fabrication. We performed thermogravimetric analysis (TGA) and differential scanning calorimetry (DSC) on both materials. Both compounds exhibited high T_d of 460 °C and high T_g of ＞ 120°C, which is favorable for OLED fabrication (Table 3).

View Article Online
DOI: 10.1039/D5SC06557G

Table 3 Thermal stability parameters and energy levels of DPXZ-PI and DPXZ-PICN.

	DPXZ-PI	DPXZ-PICN
μ_{elec}（$cm^2 \cdot V^{-1} \cdot s^{-1}$）	1.86×10^{-6}	3.78×10^{-6}
μ_{hole}（$cm^2 \cdot V^{-1} \cdot s^{-1}$）	1.56×10^{-4}	3.79×10^{-4}
T_g (℃)	＞120℃	＞120℃
T_d (℃)	460	458
HOMO(eV)	-5.08	-5.12
LUMO(eV)	-2.35	-2.30

Accordingly, we initially fabricated the non-doped OLEDs for DPXZ-PI and DPXZ-PICN with structures of ITO/HATCN (5 nm)/TAPC (25 nm)/TCTA (15 nm)/DPXZ-PI (20 nm)/TmPyPb (35 nm)/LiF (1 nm)/Al (100 nm) and ITO/HATCN (5 nm)/TAPC(30 nm)/TCTA (15 nm)/DPXZ-PICN (20 nm)/TmPyPb (30 nm)/LiF (1 nm)/Al (100 nm) respectively. As shown in Figure 4 and Table 4, The DPXZ-PI-based non-doped device achieved a maximum EQE of 9.9% with Commission Internationale de l'Eclairage (CIE) coordinate of (0.207, 0.459). With respect to the high performance among the HLCT materials-based OLEDs, we further proceeded to fabricate the doped OLEDs utilizing PhCzBCz as the host matrix, using the device structures of ITO/HATCN (5 nm)/TAPC (25 nm)/TCTA (10 nm)/PhCzBCz : DPXZ-PI/TmPyPb (35 nm)/LiF (1 nm)/Al (100 nm) and ITO/HATCN (5 nm)/TAPC (30 nm)/TCTA (10 nm)/PhCzBCz : DPXZ-PICN/TmPyPb (30 nm)/LiF (1 nm)/Al (100 nm). The DPXZ-PI doped OLED delivered a remarkable maximum EQE of 14.8%, with CIE coordinates of (0.166, 0.280). This performance represents the highest reported EQE for sky-blue-emitting OLEDs with a comparable molecular structure to date. For DPXZ-PICN, notably, despite the sharp quenching in the non-doped powder, the DPXZ-PICN-based non-doped OLED can also reach a record-setting maximum EQE of 11.67% with a blue-greenish EL, despite that the doped OLED based on DPXZ-

PICN exhibited a significant performance reduction (maximum EQE of only 7.4%)(Figure 4,Table 4). These seemingly reversed EQE results are complicated and probably be related to the electric-field regulation effect,[67]but in terms of the HLCT excited state, cyano-substitution upon DPXZ-PI does not cause much effect on the EQE, again revealing the robustness of the co-axial HLCT construction method.

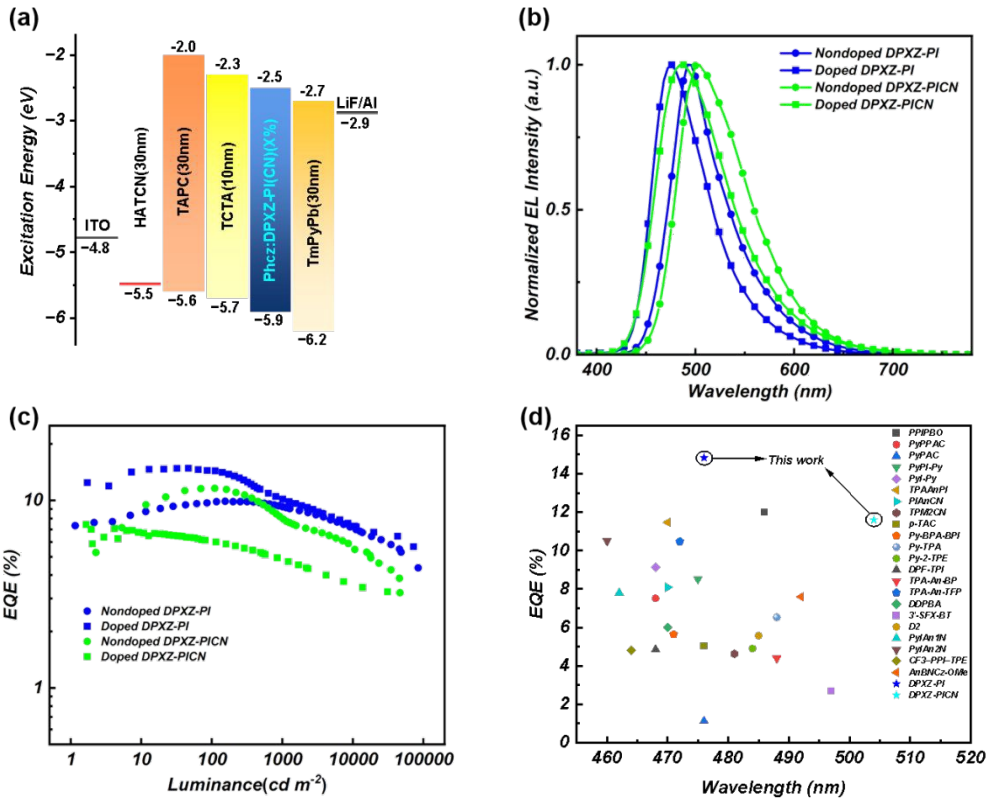

Figure 4 OLED performance of DPXZ-PI and DPXZ-PICN. (a) Schematic diagram of OLED structure (b) EL spectra (c) EQE-EL relation (d) Result comparison among the reported HLCT materials-based OLED.[68-86]

View Article Online
DOI: 10.1039/D5SC06557G

Table 4 OLED performance of DPXZ-PI and DPXZ-PICN.

Device	V_{on} (V)	LE_{max}[e] (cd/A)	PE_{max}[f] (lm/W)	CIE (x,y)	L_{max}[g] (cd/m^2)	EQE_{max} (%)	PLQY (%)	Roll-off[h] (%)
1[a]	2.8	25.59	22.3	(0.207,0.459)	84225	9.9	100	N. A./6.3
2[b]	3.2	29.22	25.90	(0.166,0.280)	72406	14.8	81.7	2.6/31.8
3[c]	3	34.19	30.69	(0.256,0.535)	46519	11.6	30.2	N. A./31.4
4[d]	3.8	17.99	14.87	(0.203,0.376)	31998	7.4	83.9	18.4/34.8

[a] Non-doped OLED of DPXZ-PI. [b] Doped OLED of DPXZ-PI. [c] Non-doped OLED of DPXZ-PICN. [d] Doped OLED of DPXZ-PICN. [e] maximum luminescent efficiency. [f] maximum powder efficiency. [g] maximum luminescence. [h] Efficiency roll-off recorded at luminescence of 100 cd/m^2 and 1000 cd/m^2, N. A. means no efficiency roll-off or minus efficiency roll-off is recorded at 100 cd/m^2.

2. 4 Mechanism of Exciton Utilization in OLED

Considering the high EQE of the non-doped OLED and the doped OLED of DPXZ-PI and DPXZ-PICN, the EUEs of their respective OLEDs would no doubt exceeded the spin-statistic limit of 25%, which can be assigned to their hRISC pathway from the LE state T_4 to the HLCT state S_1 that originated from the DPXZ-PI backbone.[87] To further verify the "hot-exciton" channel in DPXZ-PI and DPXZ-PICN, we conduct the temperature-dependent photoluminescence (PL) spectra and lifetime measurements on both materials. First, the PL intensity of both DPXZ-PI and DPXZ-PICN initially decreased and subsequently increased with rising temperature (Figure 5a).[88] The initial PL decrease before 150 ℃ can be assigned to the activated molecular motion with temperature increasing, and the subsequent PL increase originates from a temperature-activated RISC process. This mechanism is further corroborated by the temperature-dependent lifetime results. In Figure 5b, significant millisecond lifetime species can be observed at the time window of 40 ms, and extra lifetime species can further be

observed at the temperature range of > 80 K, which is consistent to our previous work on the D-π-A HLCT materials, [43]that is, the extra lifetime species is critically linked to the thermally activated reversed innerconversion (RIC). To validate the RIC pathway, we carried out ultrafast absorption spectroscopy using the $Ir(ppy)_3$ sensitized solution of DPXZ-PI and DPXZ-PICN (Figure S17). As shown in Figure 5c, for both DPXZ-PI and DPXZ-PICN sensitized solution, broad, stationary absorption bands that remain invariant over time can be observed in the near-infrared (NIR) region, corresponding to the $T_1 \rightarrow T_n$ transition energies of 1.1787 eV and 1.1376 eV, respectively. Referencing the energy level diagrams in Figure 1a, the $T_1 \rightarrow T_n$ transitions revealed by the ultrafast absorptions of DPXZ-PI and DPXZ-PICN can be assigned to their $T_1 \rightarrow T_4$ transitions, which also comply with the El-Sayed rule judging from the similar $\pi \rightarrow \pi^*$ transition pattern of T_1 and T_4 (Figure S2).[89-92]

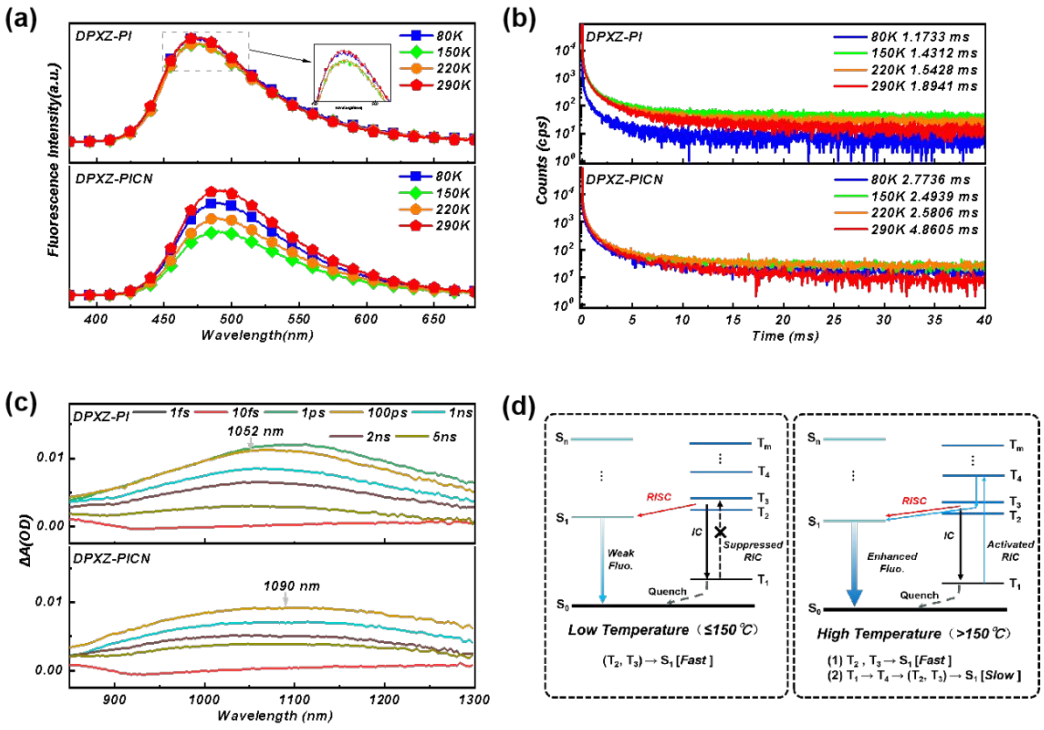

Figure 5 (a) Temperature dependent PL spectra of DPXZ-PI and DPXZ-PICN (b) Temperature dependent lifetime of DPXZ-PI and DPXZ-PICN within time window of 40 ms (c) Ultrafast absorption of DPXZ-PI and DPXZ-PICN with $Ir(ppy)_3$ as sensitizer (d) Schematic diagram of the hRISC channel in DPXZ-PI and DPXZ-PICN.The

View Article Online
DOI: 10.1039/D5SC06557G

concentration of the diluted solutions is 1×10^{-5} M.

Table 5 Summary of the lifetimes of DPXZ-PI and DPXZ-PICN.

Temperature (K)	DPXZ-PI					DPXZ-PICN				
	τ_p(ns)	τ_d(ms)				τ_p(ns)	τ_d(ms)			
	τ(ns)	τ_1[ms]/Rel%	τ_2[ms]/Rel%	τ_3[ms]/Rel%	τ_{aver}[ms]	τ(ns)	τ_1[ms]/Rel%	τ_2[ms]/Rel%	τ_3[ms]/Rel%	τ_{aver}[ms]
80	3.895	0.211/43.82%	1.924/56.18%	-	1.173	4.736	0.659/58.72%	5.858/41.28%	-	2.774
150	3.919	0.059/15.05%	0.482/49.33%	3.325/35.62%	1.431	4.758	0.332/30.52%	1.730/41.26%	18.91/28.23%	6.153
220	3.995	0.076/17.93%	0.558/49.19%	3.817/32.88%	1.543	4.814	0.325/29.09%	1.822/40.07%	22.37/30.83%	7.722
290	3.997	0.111/24.23%	0.753/48.02%	5.427/27.75%	1.894	4.833	0.391/31.65%	2.148/36.86%	20.45/31.49%	7.355

3. Conclusion

In summary, we reported two highly efficient electro-fluorescent materials DPXZ-PI and DPXZ-PICN with the excited state design of co-axial HLCT, which is theoretically and experimentally investigated. The matching of strong donor and weak acceptor helps forming more orbit-overlap and higher PLQY while maintain the CT character for exceeding EUE, which is the key reason for the high EQE of 14.8% for the doped OLED of DPXZ-PI. Also, the co-axial HLCT state is also robust even upon substitution of strong acceptor, which enables the 11.6% EQE of the non-doped OLED of DPXZ-PICN. With the advantage of high PLQY and EUE, the method of co-axial HLCT is expected to be the novel method for the design of cost-effective and easily scalable next-generation electro-fluorescent materials.

Data availability statement

All relevant data are either included in the main text or in the supporting information. Additional data are also available from the authors on request.

Acknowledgements

This work is supported by the National Natural Science Foundation of China

View Article Online
DOI: 10.1039/D5SC06557G

(51803071, 52303230), the Taishan Scholar Constructive Engineering Foundation of Shandong Province of China (No. tsqn202211164) and the innovative research project of the state key laboratory of supramolecular structure and materials. The authors gratefully acknowledgement HZWTECH for providing computation facilities and discussions.

References

[1] M. A. Baldo, D. F. O'Brien, Y. You, A. Shoustikov, S. Sibley, M. E. Thompson, S. R. Forrest, *Nature* **1998**, *395*, 151-154.

[2] D. Y. Kondakov, T. D. Pawlik, T. K. Hatwar, J. P. Spindler, *Journal of Applied Physics* **2009**, *106*.

[3] C. J. Chiang, A. Kimyonok, M. K. Etherington, G. C. Griffiths, V. Jankus, F. Turksoy, A. P. Monkman, *Advanced Functional Materials* **2013**, *23*, 739-746.

[4] L. Xing, Z.-L. Zhu, J. He, Z. Qiu, Z. Yang, D. Lin, W.-C. Chen, Q. Yang, S. Ji, Y. Huo, *Chemical Engineering Journal* **2021**, *421*, 127748.

[5] H. Lim, S. J. Woo, Y. H. Ha, Y. H. Kim, J. J. Kim, *Advanced Materials* **2022**, *34*, 2100161.

[6] J. Qin, X. Qiao, S. Xiao, D. Yang, Y. Dai, J. Chen, Q. Sun, D. Ma, *Chemical Science* **2025**, *16*, 3536-3543.

[7] H. Uoyama, K. Goushi, K. Shizu, H. Nomura, C. Adachi, *Nature* **2012**, *492*, 234-238.

[8] G. Zhao, D. Liu, P. Wang, X. Huang, H. Chen, Y. Zhang, D. Zhang, W. Jiang, Y. Sun, L. Duan, *Angewandte Chemie* **2022**, *134*, e202212861.

[9] L. Liang, C. Qu, X. Fan, K. Ye, Y. Zhang, Z. Zhang, L. Duan, Y. Wang, *Angewandte Chemie International Edition* **2024**, *63*, e202316710.

[10] H. Wang, J. X. Chen, Y. Z. Shi, X. Zhang, L. Zhou, X. Y. Hao, J. Yu, K. Wang, X. H. Zhang, *Advanced Materials* **2024**, *36*, 2307725.

[11] T. Huang, Q. Wang, H. Zhang, Y. Zhang, G. Zhan, D. Zhang, L. Duan, *Nature Photonics* **2024**, *18*, 516-523.

[12] Y. X. Hu, J. Miao, T. Hua, Z. Huang, Y. Qi, Y. Zou, Y. Qiu, H. Xia, H. Liu, X. Cao, *Nature Photonics* **2022**, *16*, 803-810.

[13] Z. Ma, Y. Wang, J. Bian, X. Long, G. Li, Z. Mao, Z. Yang, J. Zhao, Z. Chi, *Chemical Engineering Journal* **2025**, 165337.

[14] F. Liu, Z. Su, Z. Cheng, D. Chen, Y. Xu, Y. Yan, W. Dong, L. Wan, E. Zysman-Colman, P. Lu, *Angewandte Chemie International Edition* **2025**, e202511866.

[15] D. Barman, Y. Tsuchiya, C. Adachi, *Nature Communications* **2025**, *16*, 5023.

[16] Y. Chiba, K. Hoshi, G. Yamda, H. Nemma, R. Otomo, D. Jiang, N. Meguro, H. Katagiri, J. Kido, H. Sasabe, *Advanced Functional Materials* **2025**, 2425759.

[17] D. Zhang, L. Duan, *Nature Photonics* **2021**, *15*, 173-174.

[18] T. Fan, C. Qu, L. Duan, Y. Zhang, *National Science Review* **2025**, nwaf250.

[19] X. Zeng, X. Luo, G. Meng, X. Wang, D. Zhang, L. Duan, *Angewandte Chemie International Edition* **2025**, *64*, e202423670.

[20] B. Liu, Z. Li, D. Li, L. Wu, T. Wang, D. Liu, S.-J. Su, W. Li, Z. Ge, *Chemical Engineering Journal* **2025**, 166027.

[21] H. J. Tan, J. L. Liu, J. R. Yu, G. X. Yang, X. Q. Gao, B. Wang, Z. Q. Long, Q. X. Tong, J. X. Jian, S. J. Su, *Advanced Functional Materials* **2025**, e11296.

[22] Z. Chen, Z. Li, Y. Tian, D. Liu, Z. Yang, M. Li, S. J. Su, *Angewandte Chemie* **2025**, e202507626.

[23] Q. Wang, L. Yuan, C. Qu, T. Huang, X. Song, Y. Xu, Y. X. Zheng, Y. Wang, *Advanced Materials* **2023**, *35*, 2305125.

[24] Y. Feng, X. Zhuang, Y. Xu, J. Xue, C. Qu, Q. Wang, Y. Liu, Y. Wang, *Chemical Engineering Journal* **2023**, *478*, 147123.

[25] T. Yang, J. Liang, Y. Cui, Z. Li, X. Peng, S. J. Su, Y. Wang, C. Li, *Advanced Optical Materials* **2023**, *11*, 2201191.

[26] J. Liu, Z. Bin, D. Yang, D. Ma, J. You, *Chemical Engineering Journal* **2023**, *466*, 142910.

[27] W. Han, J. Liu, C. Ran, Z. Huang, G. Gao, J. You, Z. Bin, *Angewandte Chemie* **2023**, *135*, e202312297.

[28] A. Luo, Y. Bao, J. Liu, Y. Yang, Y. Deng, J. You, Z. Bin, *Angewandte Chemie International Edition* **2024**, *63*, e202411464.

[29] H. Wu, Y.-Z. Shi, M.-Y. Li, X.-C. Fan, F. Huang, K. Wang, J. Yu, X.-H. Zhang, *Chemical Engineering Journal* **2024**, *480*, 147977.

[30] X. S. Zhong, J. Q. Xi, J. J. Hu, L. Yuan, Y. X. Zheng, *Advanced Optical Materials* **2025**, *13*, 2500395.

[31] M. Gong, X. Guo, L. Yuan, H. Jiang, G. Zeng, W.-H. Zheng, Y.-X. Zheng, *Chemical Engineering Journal* **2025**, *505*, 159719.

[32] W. Li, Y. Pan, R. Xiao, Q. Peng, S. Zhang, D. Ma, F. Li, F. Shen, Y. Wang, B. Yang, *Advanced Functional Materials* **2014**, *24*, 1609-1614.

[33] S. Du, M. Luo, D. Li, L. Lyu, W. Li, M. Zhao, Z. Wang, J. Zhang, D. Liu, Y. Li, *Advanced Materials* **2023**, *35*, 2303304.

[34] W. Wang, J. Bian, K. Chen, C. Li, Y. Long, H. Huang, L. Jiang, J. Zhao, S. Liu, Z. Chi, *Angewandte Chemie International Edition* **2024**, *63*, e202318782.

[35] G. Li, K. Xu, J. Zheng, X. Fang, W. Lou, F. Zhan, C. Deng, Y.-F. Yang, Q. Zhang, Y. She, *Journal of the American Chemical Society* **2024**, *146*, 1667-1680.

[36] C. Du, H. Liu, Z. Cheng, S. Zhang, Z. Qu, D. Yang, X. Qiao, Z. Zhao, P. Lu, *Advanced Functional Materials* **2023**, *33*, 2304854.

[37] Z. Gao, G. Cheng, F. Shen, S. Zhang, Y. Zhang, P. Lu, Y. Ma, *Laser & Photonics Reviews* **2014**, *8*, L6-L10.

[38] R. Tang, H. Guo, L. Gong, Y. Chen, Y. Duan, S. Wang, Z. Chen, F. X. Luo, L. Xiao, *Advanced Optical Materials* **2025**, *13*, 2500726.

[39] M. Xie, Y. Zhou, L. Zhang, J. Song, C. Ma, Q. Sun, S.-T. Zhang, W. Yang, S. Xue, *Chemical Engineering Journal* **2024**, *500*, 156905.

[40] M. Sun, C. Ma, M. Xie, L. Chu, Q. Sun, W. Yang, S. Xue, *Chemical Engineering Journal* **2024**, *480*, 148107.

[41] M. Sun, R. Wang, C. Ma, Y. Zhou, X. Wang, L. Chu, W. Yang, S. Xue, *Chemical Engineering Journal* **2025**, *507*, 160436.

[42] Y. Gao, Y. Deng, Y. Lv, X. Tian, H. Liu, S.-T. Zhang, J. Sheng, B. Yang, *Chemical Engineering Journal* **2024**, *481*, 148725.

[43] R. Wu, K. Sun, G. Shi, Y. Han, T. Gong, Y. Xu, S. T. Zhang, B. Yang, *Advanced Functional Materials* **2024**, *34*, 2403501.

[44] M. Yao, S. Men, K. Yu, J. Wei, S. T. Zhang, B. Yang, *Chemistry–A European Journal* **2025**, *31*, e202404752.

[45] S. Zhang, W. Li, L. Yao, Y. Pan, F. Shen, R. Xiao, B. Yang, Y. Ma, *Chemical Communications* **2013**, *49*, 11302-11304.

[46] W. Li, D. Liu, F. Shen, D. Ma, Z. Wang, T. Feng, Y. Xu, B. Yang, Y. Ma, *Advanced Functional Materials* **2012**, *22*, 2797-2803.

[47] S. Zhang, L. Yao, Q. Peng, W. Li, Y. Pan, R. Xiao, Y. Gao, C. Gu, Z. Wang, P. Lu, *Advanced Functional Materials* **2015**, *25*, 1755-1762.

[48] H. Noda, X.-K. Chen, H. Nakanotani, T. Hosokai, M. Miyajima, N. Notsuka, Y. Kashima, J.-L. Brédas, C. Adachi, *Nature Materials* **2019**, *18*, 1084–1090.

[49] L.-S. Cui, A. J. Gillett, S.-F. Zhang, H. Ye, Y. Liu, X.-K. Chen, Z.-S. Lin, E. W. Evans, W. K. Myers, T. K. Ronson, *Nature Photonics* **2020**, *14*, 636–642.

[50] J. Lou, X. Guo, Y. Chen, H. Zhang, D. Yang, D. Ma, B. Z. Tang, Z. Wang, *Chemical Engineering Journal* **2025**, 163817.

[51] X. K. Chen, Y. Tsuchiya, Y. Ishikawa, C. Zhong, C. Adachi, J. L. Brédas, *Advanced Materials* **2017**, *29*, 1702767.

[52] H. Noda, X.-K. Chen, H. Nakanotani, T. Hosokai, M. Miyajima, N. Notsuka, Y. Kashima, J.-L. Brédas, C. Adachi, *Nature Materials* **2019**, *18*, 1084-1090.

[53] L.-S. Cui, A. J. Gillett, S.-F. Zhang, H. Ye, Y. Liu, X.-K. Chen, Z.-S. Lin, E. W. Evans, W. K. Myers, T. K. Ronson, *Nature Photonics* **2020**, *14*, 636-642.

[54] Z. Yang, N. Qiu, X. Dong, J. Li, P. Zou, D. Yang, D. Ma, B. Z. Tang, Z. Zhao, *Advanced Optical Materials* **2024**, *12*, 2302677.

[55] M. Frisch, G. Trucks, H. B. Schlegel, G. Scuseria, M. Robb, J. Cheeseman, G. Scalmani, V. Barone, G. Petersson, H. Nakatsuji, *Inc., Wallingford CT* **2016**, *2016*.

[56] T. Lu, F. Chen, *Journal of computational chemistry* **2012**, *33*, 580-592.

[57] W. Liu, G. Hong, D. Dai, L. Li, M. Dolg, *Theoretical Chemistry Accounts* **1997**, *96*, 75-83.

[58] W. Liu, F. Wang, L. Li, *Journal of Theoretical and Computational Chemistry* **2003**, *2*, 257-272.

[59] U. Kaldor, E. Eliav, A. Landau, K. Hirao, Y. Ishikawa, *World Scientific, Singapore* **2004**, 283.

[60] Y. Zhang, B. Suo, Z. Wang, N. Zhang, Z. Li, Y. Lei, W. Zou, J. Gao, D. Peng, Z. Pu, *The Journal of Chemical Physics* **2020**, *152*.

[61] Q. Peng, Y. Yi, Z. Shuai, J. Shao, *The Journal of chemical physics* **2007**, *126*.

[62] Q. Peng, Y. Yi, Z. Shuai, J. Shao, *Journal of the American Chemical Society* **2007**, *129*, 9333-9339.

[63] Y. Niu, Q. Peng, Z. Shuai, *Science in China Series B: Chemistry* **2008**, *51*, 1153-1158.

[64] Y. Niu, Q. Peng, C. Deng, X. Gao, Z. Shuai, *The Journal of Physical Chemistry A* **2010**, *114*, 7817-7831.

[65] Q. Peng, Y. Niu, Q. Shi, X. Gao, Z. Shuai, *Journal of Chemical Theory and Computation* **2013**, *9*, 1132-1143.

[66] Z. Shuai, Q. Peng, *Physics Reports* **2014**, *537*, 123-156.

[67] H. T. Yi, S. Rangan, B. Tang, C. D. Frisbie, R. A. Bartynski, Y. N. Gartstein, V. Podzorov, *Materials Today* **2019**, *28*, 31-39.

[68] Y. Liu, H. Liu, Q. Bai, C. Du, A. Shang, D. Jiang, X. Tang, P. Lu, *ACS applied materials & interfaces* **2020**, *12*, 16715-16725.

[69] Y. Liu, X. Man, Q. Bai, H. Liu, P. Liu, Y. Fu, D. Hu, P. Lu, Y. Ma, *CCS Chemistry* **2022**, *4*, 214-227.

[70] Y. Liu, L. Yang, Q. Bai, W. Li, Y. Zhang, Y. Fu, F. Ye, *Chemical Engineering Journal* **2021**, *420*, 129939.

[71] X. Lv, M. Sun, L. Xu, R. Wang, H. Zhou, Y. Pan, S. Zhang, Q. Sun, S. Xue, W. Yang, *Chemical Science* **2020**, *11*, 5058-5065.

[72] X. Tang, Q. Bai, T. Shan, J. Li, Y. Gao, F. Liu, H. Liu, Q. Peng, B. Yang, F. Li, *Advanced Functional Materials* **2018**, *28*, 1705813.

[73] S.-T. Zhang, X. Bai, X. Li, Q. Bai, M. Wang, H. Liu, P. Lu, S.-J. Su, B. Yang, *Organic Electronics* **2019**, *75*, 105404.

[74] Z. Zhao, G. Wang, X. Luo, X. Tian, D. Zhang, S. Guo, H. Zhou, Y. Miao, J. Huang, H. Wang, *Dyes and Pigments* **2022**, *204*, 110391.

[75] B. Liu, Y. Yuan, D. He, D. Y. Huang, C. Y. Luo, Z. L. Zhu, F. Lu, Q. X. Tong, C. S. Lee, *Chemistry–A European Journal* **2016**, *22*, 12130-12137.

[76] J. Zeng, N. Qiu, J. Zhang, X. Wang, C. Redshaw, X. Feng, J. W. Lam, Z. Zhao, B. Z. Tang, *Advanced Optical Materials* **2022**, *10*, 2200917.

[77] Y. Yuan, J.-X. Chen, F. Lu, Q.-X. Tong, Q.-D. Yang, H.-W. Mo, T.-W. Ng, F.-L. Wong, Z.-Q. Guo, J. Ye, *Chemistry of Materials* **2013**, *25*, 4957-4965.

[78] X. Liang, Z. Wang, L. Wang, M. Hanif, D. Hu, S. Su, Z. Xie, Y. Gao, B. Yang, Y. Ma, *Chinese Journal of Chemistry* **2017**, *35*, 1559-1568.

[79] J. Zhang, Y. Zhao, H. Xu, D. Zhang, Y. Miao, R. Shinar, J. Shinar, H. Wang, B. Xu, Y. Wu, *Journal of Materials Chemistry C* **2019**, *7*, 10810-10817.

[80] J. Jayabharathi, J. Anudeebhana, V. Thanikachalam, S. Sivaraj, *RSC advances* **2020**, *10*, 8866-8879.

[81] W. Cui, C. Liu, X. Chao, M. Xie, Q. Sun, D. Liu, Y. Pan, S. T. Zhang, S. Xue, W. Yang, *Advanced Optical Materials* **2023**, *11*, 2202947.

[82] E.-S. Zhou, Q. Chen, X. Long, C.-S. Li, Z.-W. Mao, B.-Y. Ren, G. Xiong, Y.-G. Sun, G. Xie, *Journal of Luminescence* **2025**, 121279.

[83] C. Ma, M. Sun, Y. Zhou, L. Chu, J. Song, L. Zhang, Q. Sun, W. Yang, S. Xue, *Dyes and Pigments* **2025**, *235*, 112647.

[84] K. Chen, Q. Luo, Y. Du, Y. Peng, X. Li, H. Xu, Y. Miao, H. Wang, R. Chen, J. Yu, *Chemical Engineering Journal* **2025**, *509*, 161133.

[85] H. Ma, X. Niu, W. Qu, Z. Feng, T. Ma, Y. Liu, S. Zhu, *Journal of Materials Chemistry C* **2025**.

[86] J. Lin, R. Wang, D. Hu, Z. Lu, Y. Zhang, Z. Ye, Y. Huo, S. Ji, *Journal of Materials Chemistry C* **2025**, *13*, 6041-6051.

DOI: 10.1039/D5SC06557G

[87] W. Li, Y. Pan, L. Yao, H. Liu, S. Zhang, C. Wang, F. Shen, P. Lu, B. Yang, Y. Ma, *Advanced Optical Materials* **2014**, *2*, 892-901.

[88] C. Zhou, D. Cong, Y. Gao, H. Liu, J. Li, S. Zhang, Q. Su, Q. Wu, B. Yang, *The Journal of Physical Chemistry C* **2018**, *122*, 18376-18382.

[89] G. Farias, C. A. Salla, M. Aydemir, L. Sturm, P. Dechambenoit, F. Durola, B. de Souza, H. Bock, A. P. Monkman, I. H. Bechtold, *Chemical Science* **2021**, *12*, 15116-15127.

[90] G. Jiang, Q. Li, A. Lv, L. Liu, J. Gong, H. Ma, J. Wang, B. Z. Tang, *Journal of Materials Chemistry C* **2022**, *10*, 13797-13804.

[91] J. Yu, Z. Sun, H. Ma, C. Wang, W. Huang, Z. He, W. Wu, H. Hu, W. Zhao, W. H. Zhu, *Angewandte Chemie International Edition* **2023**, *62*, e202316647.

[92] X. Yang, S. Wang, K. Sun, H. Liu, M. Ma, S. T. Zhang, B. Yang, *Angewandte Chemie International Edition* **2023**, *62*, e202306475.

View Article Online
DOI: 10.1039/D5SC06557G

View Article Online
DOI: 10.1039/D5SC06557G

All relevant data are either included in the main text or in the supporting information. Additional data are also available from the authors on request.